

LETTER

Compact spoof surface plasmonic waveguide with controllable cutoff frequency and wide stop band

To cite this article: Bocong Ren *et al* 2021 *Appl. Phys. Express* **14** 024002

View the [article online](#) for updates and enhancements.

You may also like

- [Effective bandpass filtering for spoof surface plasmon polariton transmission lines](#)
Shaowei Liao, Chu Qi and Quan Xue
- [Active spoof plasmonics: from design to applications](#)
Yi Ren, Jingjing Zhang, Xinxin Gao et al.
- [Bandwidth enhancement of a half-mode substrate integrated waveguide filtering power divider using spoof surface plasmon polariton](#)
Ali-Reza Moznebi and Kambiz Afroz



Compact spoof surface plasmonic waveguide with controllable cutoff frequency and wide stop band

Bocong Ren, Lei Zhang, Jiangfeng Lu, Yuchen Yang, Weiwen Li^{*} , and Baoping Zhang^{*}

Department of Electronic Engineering, Xiamen University, Xiamen 361005, People's Republic of China

^{*}E-mail: wwl@xmu.edu.cn; bzhang@xmu.edu.cn

Received December 27, 2020; revised January 5, 2021; accepted January 12, 2021; published online January 28, 2021

To adjust the transmission band while keeping the width of a spoof surface plasmon polariton (SSPP) waveguide unchanged, periodic cells with T-shaped conductor branches on both sides are used. By controlling the top lateral strips of branches, the adjustable range of cutoff frequencies can reach approximately 3.5 GHz. Thus, compromised regulation of the field confinement and transmission loss is easily achieved, improving the transmission performance of SSPP modes. By loading open conductor rings onto T-shaped branches to construct a split ring resonator (SRR), a band-rejection filter is realized. When multiple SRRs with gradient lengths are loaded onto one side of the SSPP waveguide, a broad stop band with a relative bandwidth of 18% is achieved. The proposed structures are also advantageous for the miniaturization of microwave circuits.

© 2021 The Japan Society of Applied Physics

Surface plasmon polaritons (SPPs) are strongly bound surface waves propagating along the conductor–dielectric interface due to the collective oscillation between light waves and metal electrons.^{1,2)} However, in the microwave region, metal behaves as a perfect electric conductor (PEC).³⁾ Even though, for example, Zenneck waves can propagate on the metal interface, they are distributed in the medium at hundreds of wavelengths and show poor confinement.⁴⁾

Fortunately, by introducing periodic holes or grooves into the metal's surface, the equivalent plasma frequency can be effectively reduced and spoof surface plasmon polaritons (SSPPs) are realized in the microwave band, which have similar characteristics to SPPs.⁵⁾ In fact, holes of sub-wavelength size periodically distributed across the surface significantly enhance the penetration of electromagnetic (EM) waves in metal and improve the field matching between the metal and the medium, thereby realizing the confinement of EM waves on a sub-wavelength scale.⁶⁾ Because the transmission frequency in structured waveguides is much lower than the plasma frequency of metal, SSPP modes have small losses. Meanwhile, the dispersion characteristics of SSPP modes can be flexibly controlled by changing the structural parameters to obtain adjustable or reconfigurable microwave components and circuits.^{7–10)}

Planar SSPP waveguides have drawn great attention for the miniaturization of microwave circuits. A thin SSPP structure can be manufactured by the etching of microwave circuit boards or the planar lithography of terahertz devices.^{11,12)} Conformal structures can be realized using flexible circuit boards, to guide SSPP modes without affecting the transmission characteristics.¹³⁾ The most common periodic cell is an H-shaped structure.¹⁴⁾ However, its asymptotic frequency is usually high and to enhance the confinement of SSPP modes, the height of the H-shaped units has to be increased, which harms device miniaturization.¹⁵⁾ To reduce the cutoff frequency while keeping the width of the SSPP waveguide constant, a periodic structure with T-shaped branches is proposed in this paper. The asymptotic frequency of this periodic cell can be effectively controlled by regulating the length of its top conductive strips. Furthermore, by loading multiple open loops onto T-shaped branches on one side of SSPP waveguide, a broad stop band can be achieved without a significant impact to the passband performance.

The periodic cell with T-shaped branches is formed by symmetrically loading lateral conductor strips onto the arm tops of an H-shaped unit as shown in Fig. 1(c). Specifically, it is fabricated on an F4BM microwave substrate with a permittivity of 2.2, a loss tangent of 0.01, and a thickness of 0.8 mm. For it to work in the microwave band, a period of $p = 5.0$ mm and a central conductor width of $H = 5.0$ mm are used. Meanwhile, the height of the vertical branch is $h = 4.0$ mm, and its width is $f1 = 0.8$ mm. The symmetrical lateral strips at the tops have a unilateral length of $e = 1.0$ mm and a width of $f2 = 0.3$ mm.

The dispersion characteristics are mostly affected by the groove depth and period of the SSPP waveguide based on the H-shaped cell.^{14,16)} Thus, for the proposed structure, the influence of the branch height h and lateral strip length e of the unit are mainly analyzed using the eigenmode expansion method. The simulation results are shown in Fig. 2, where the straight line is the light cone in the medium. Since the wave vector changes as a gradient with h values at the same frequency, a transition between the traditional transmission line and the guided wave structure of the SSPP modes can be achieved by gradually varying the branch height h . In the case of $h = 4.0$ mm, the asymptotic frequency with strong mode confinement is 9.7 GHz.

At $e = 0.0$ mm, that is, the periodic unit returns to the traditional H-shaped structure, the asymptotic frequency is 11.7 GHz, which is nearly 2 GHz higher than that with a T-shaped unit of $e = 1.0$ mm. As e increases, the asymptotic frequency decreases, which indicates that at a given unit height, the T-shaped periodic cell can have strong SSPP confinement. In fact, due to the strong restraining ability of electric fields at $e = 2.0$ mm, the SSPP mode begins to exhibit a negative group velocity.

As shown in Fig. 2, SSPP modes are lowpass slow waves. As T-shaped branches are applied, the cutoff frequency of the SSPP waveguide is strongly affected by the length of the top strips. Since loading lateral strips can equivalently increase the groove depth, it is possible to regulate the transmission feature of the SSPP waveguide by adjusting the strip length e , without increasing the waveguide width.

The overall structure of the SSPP waveguide is shown in Fig. 1(a), and consists of three different regions: coplanar waveguide (CPW) ports as part I, gradual transition segments as part II, and the SSPP transmission structure as part III. For

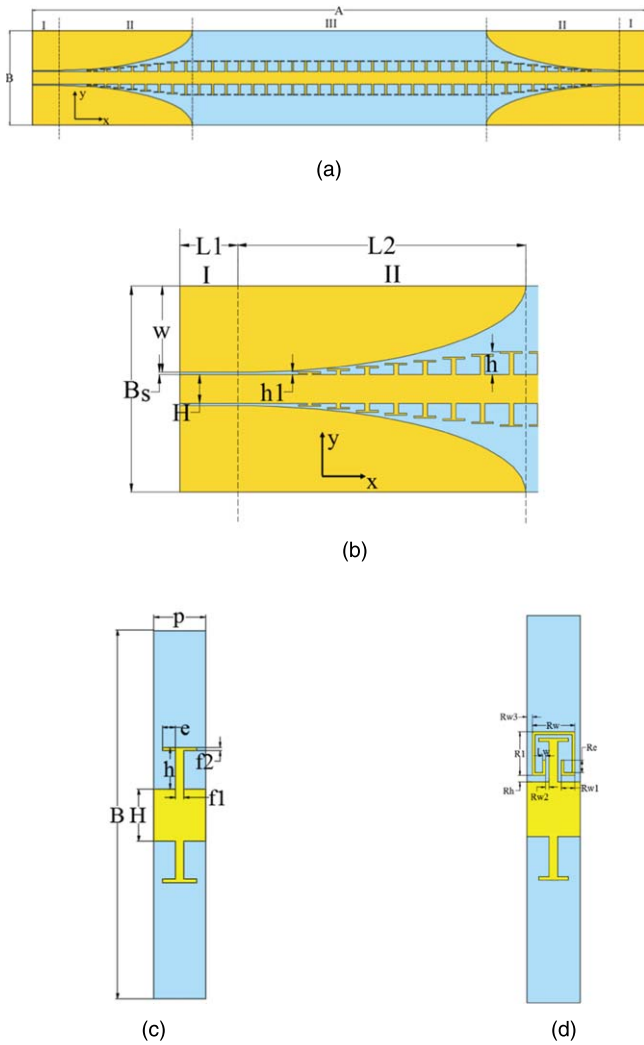


Fig. 1. (Color online) SSPP waveguide loaded with T-shaped branches, where yellow represents the metal layer and light blue represents the dielectric substrate. (a) The overall structure of the SSPP waveguide, (b) partially enlarged structure for the feed port, (c) periodic unit structure, and (d) periodic unit with a split ring.

the CPW of part I, as shown in Fig. 1(b), the width of the central conductor strips is $H = 5.0$ mm and the length is $L1 = 10.0$ mm. The width of the ground plane on one side is $w = 15.0$ mm and the slot width is $s = 0.4$ mm. This CPW has a characteristic impedance of 50Ω and can be directly terminated with SMA (Sub-Miniature-A) connectors.

The transition segments of part II include a central conductor strip for wave-vector matching and two symmetrical 1/4-elliptical ground plates for mode conversion. As shown in Fig. 1(b), the length of region II is $L2 = 50.0$ mm and 8 pairs of T-shaped branches are loaded on both sides of the conductor strip. The height of the branches gradually increases from $h1 = 0.5$ mm to $h = 4.0$ mm in equal steps, while the length of the top transverse conductor is kept at $e = 1.0$ mm. Meanwhile, the semi-minor and semi-major axes of the ground plane are $w = 15.0$ mm and $L2 = 50.0$ mm, respectively.

Part III is the stable transmission region of the SSPP mode, which contains 22 periodic units with T-shaped branches and has a total length of 110.0 mm. Thus, the length of the whole waveguide is $A = 230.0$ mm and the width is $B = 35.8$ mm. According to the coordinate system shown in Fig. 1, the

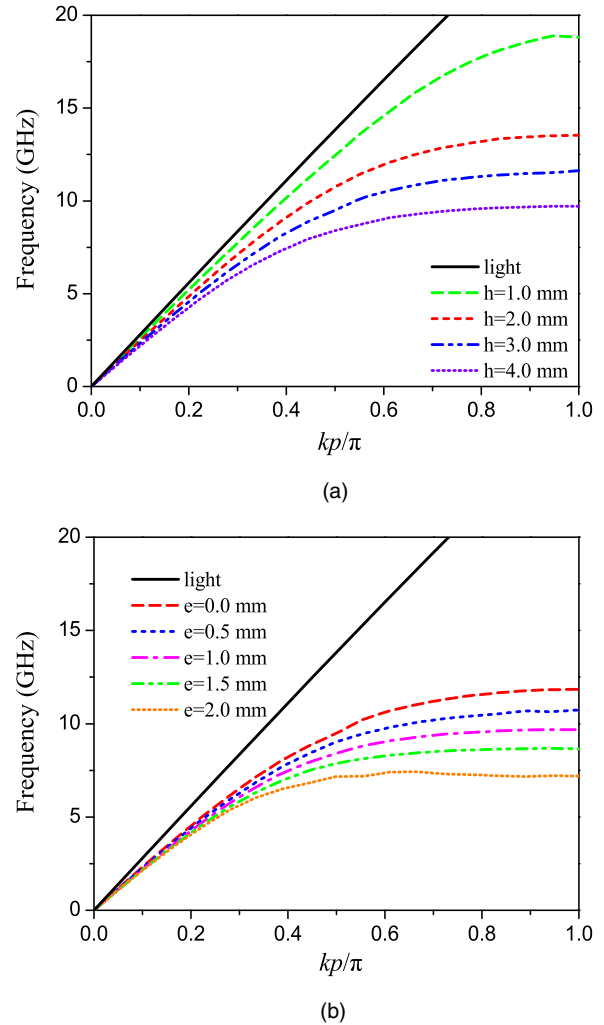


Fig. 2. (Color online) For the proposed periodic unit, the influence of the T-shaped branch (a) height h for the case of $p = 5.0$ mm, $H = 5.0$ mm, $e = 1.0$ mm and (b) top strip length e in the case of $p = 5.0$ mm, $H = 5.0$ mm, $h = 4.0$ mm on dispersion characteristics.

propagation direction of the waveguide is along the x axis and the direction normal to waveguide plane is along the z axis. The inset of Fig. 3 shows the waveguide prototype fabricated by the etching method.

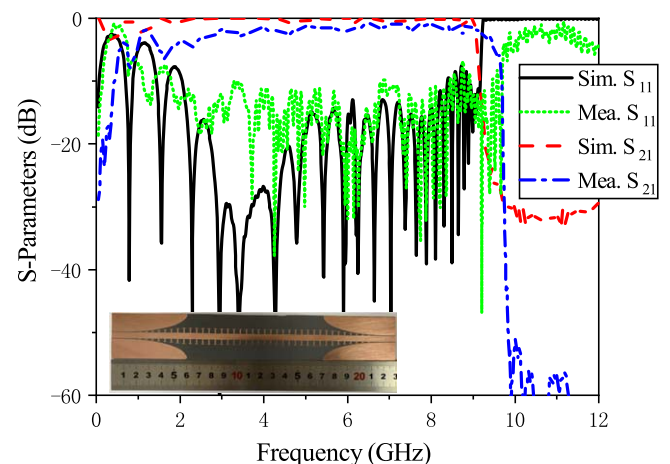


Fig. 3. (Color online) Transmission characteristics of the proposed SSPP waveguide.

The simulated and measured results of the scattering parameters for the proposed SSPP waveguide are shown in Fig. 3. From the simulation results, it can be seen that the waveguide has excellent low pass transmission performance and that the S_{21} value drops rapidly near the cutoff frequency, which is close to the asymptotic frequency of the dispersion curve. At the low-frequency end (less than 1.9 GHz), the fluctuation of the S_{21} value increases, and S_{11} significantly deteriorates. The reason is that electromagnetic waves at lower frequencies cannot be adequately confined to the metal's surface and they work as Zenneck waves. Considering the medium loss, the measured results are basically consistent with the simulated results. However, due to manufacturing errors, the measured cutoff frequency is slightly shifted towards the high-frequency end.

As shown in Fig. 2(b), the top lateral strips of the T-shaped branches have a large impact on the asymptotic frequency. Therefore, the transmission band regulation of the SSPP waveguide can be realized without increasing the overall conductor width. The simulated transmission performance for different e values is shown in Fig. 4. It can be seen that the

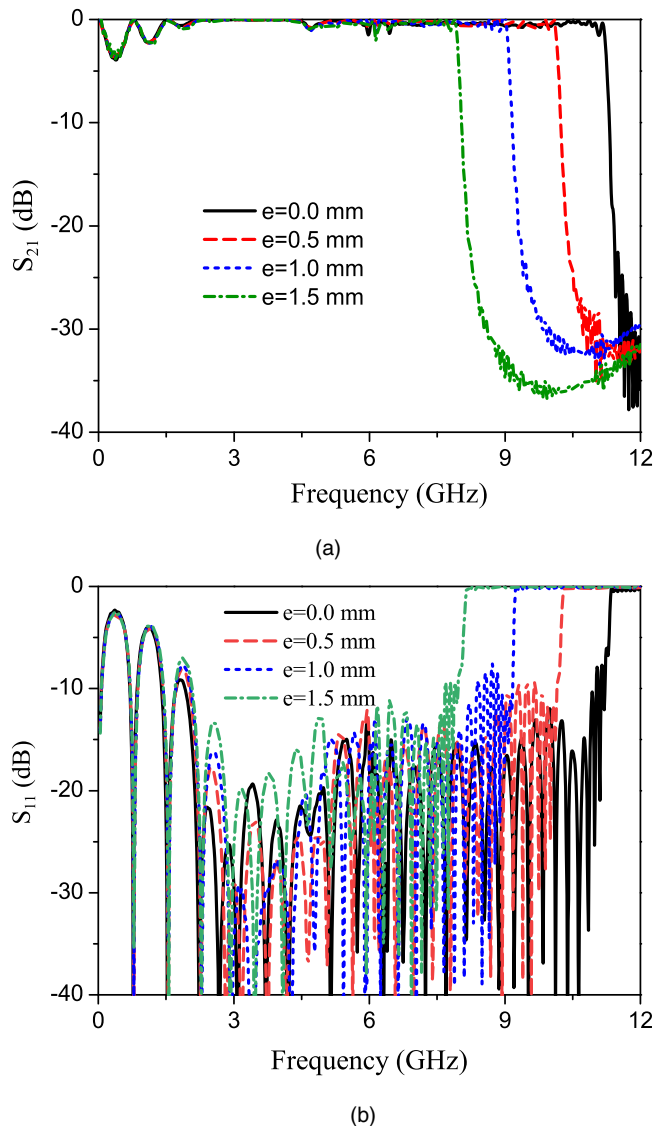


Fig. 4. (Color online) The influence of the top lateral conductor of the T-shaped branches on the scattering characteristics. (a) Transmission coefficient and (b) reflection coefficient.

cutoff frequency decreases with increasing e values, while the scattering parameters below the cutoff frequency basically remain unchanged.

For a given period $p = 5.0$ mm, the maximum change of e is 2.1 mm. However, if the top conductor strips of two periodic cells are too close, the transmission band performance deteriorates due to coupling influence. Thus, the maximum change of e is taken to be 1.5 mm. As $e = 0.0$ mm, the cutoff frequency is about 11.4 GHz. This confirms that the controllable range of cutoff frequencies can reach 3.5 GHz or so.

Conductor loss, dielectric loss, and radiation loss are the main factors causing energy dissipation in microwave transmission lines.^{17–19)} Due to the strong confinement of SSPPs, the energy dissipation caused by radiation can be ignored. Since a good conductor is used, the conductor loss caused by the collision of metal electrons can also be neglected. Thus, dielectric loss is the main loss that needs to be considered. In this case, an SSPP waveguide with stronger field localization will have a higher transmission loss.

As the loss tangents of the dielectric substrate are 0.1 and 0.01, respectively, the distributions of the electric field component E_z on the conductor's surface at 2.0, 6.0, and 8.0 GHz are shown in Fig. 5. It can be seen that for the substrate with a loss tangent of 0.1, the E_z amplitude at 2.0 GHz is almost the same on both sides of the waveguide while it is fed from the left port. At 6.0 GHz, however, the amplitude decreases from a maximum of 1463 V m^{-1} to a minimum of 628 V m^{-1} and at 8.0 GHz this reduction is even greater. Obviously, as the frequency increases, the confinement of the SSPP modes is enhanced and the energy loss also increases. For the substrate with a loss tangent of 0.01, this amplitude change is relatively small over the entire frequency band.

Therefore, in order to realize long-range transmission, both the confinement and the loss of SSPP modes should be taken into account. The SSPP waveguides can show low transmission losses at the frequency band with weak field confinement. That is, the cutoff frequency should be appropriately increased to reduce the transmission loss. By adjusting the lengths of the top conductor strips of the proposed waveguide, SSPP modes with less attenuation can be obtained in the desired frequency band.

Split ring resonators (SRRs) are constructed by nesting two metal rings with opposite openings. As magnetic fields pass vertically through the ring plane, an induced current is generated in the metal ring and coupling capacitances are formed between the inner and outer rings and at the opening of the ring. Therefore, a SRR can be equivalent to an LC circuit, and its resonant frequency can be controlled by the SRR's structural parameters.^{20–22)} In fact, when acting as a band-stopped cell, an SRR has equivalent negative permeability and positive permittivity, so only evanescent waves can be propagated by it.

If a split ring is loaded onto the T-shaped branch used as an inner ring, a compact SRR is formed and thus a stop band is generated in the SSPP waveguide. The proposed band-rejection unit is shown in Fig. 1(d). For this SRR, there is a strong capacitive coupling between the conductor strip bent upward at the opening of outer ring and the vertical conductor of the T-shaped branch. By adjusting the length

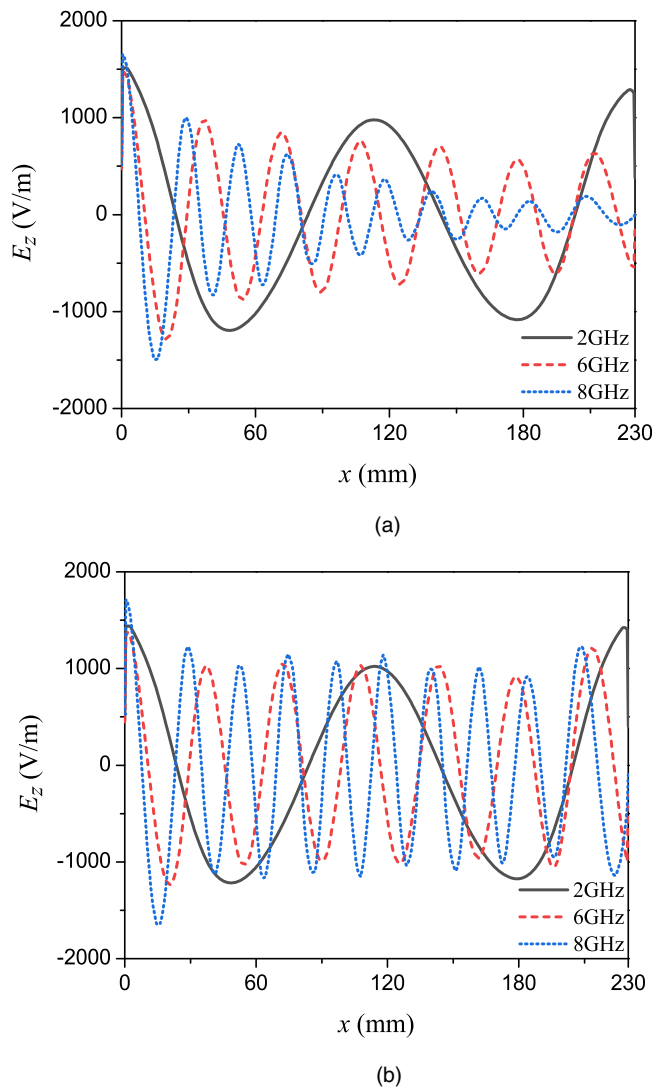


Fig. 5. (Color online) Distributions of field component E_z in the propagation direction for different dielectric losses. (a) Loss tangent of 0.1 and (b) loss tangent of 0.01.

of bent conductor Re , the circumference of the outer ring is changed and the coupling capacitance is also controlled. Thus, it can be used to achieve effective regulation of the stop band, while keeping the overall height of the rejection unit unchanged.

To match the T-shaped branch of the SSPP waveguide, the horizontal width of the outer ring, as shown in Fig. 1(d), is $Rw = 4.0$ mm, the vertical height is $Rl = 4.0$ mm, and the width of the entire ring conductor strip is $Lw = 0.25$ mm. The distance between the bent conductor at the opening and the outer conductor of the ring is $Rw1 = 1.25$ mm, the distance from the T-shaped branch vertical conductor is $Rw2 = 0.35$ mm, and the length of the bent conductor $Re = 1.5$ mm. The distance between the outer conductor of the ring and the period boundary is $Rw3 = 0.5$ mm, and the distance between the lower conductor and the central metal strip is $Rh = 0.6$ mm.

On one side of the eleventh periodic unit in area III of the SSPP waveguide, one such outer split ring is loaded to generate a stop band in the SSPP waveguide. Its structural prototype is shown in the inset of Fig. 6. The simulated and test results of the S -parameters are also shown in Fig. 6. We

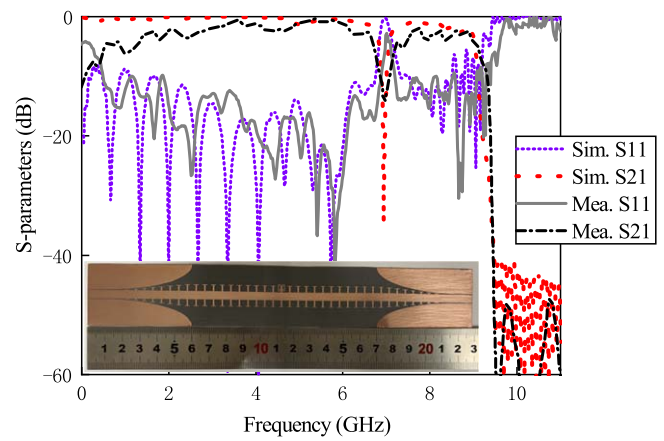


Fig. 6. (Color online) Measured and simulated scattering parameters for the SSPP waveguide loaded with a single SRR.

can observe that the simulation cutoff frequency of the SSPP waveguide is about 9.1 GHz. Due to the introduction of a single SRR, the S_{21} within 6.9–7.0 GHz is less than -10 dB and the relative bandwidth is 1.4%. The loaded SRR has little adverse impact on the passband performance. The measured results are basically consistent with the simulated results. However, due to dielectric loss and processing and test errors, the measured performance has somewhat deteriorated, especially transmission at the lower-frequency end. Meanwhile, the scattering parameters at both sides of the narrow rejection band change relatively slowly.

The T-shaped branches in the SSPP waveguide are symmetrically distributed, so loading only one SRR would destroy the structural symmetry. Thus, a waveguide with SRRs on both sides is envisaged to broaden the stop band. The simulation S -parameters (not shown here for simplicity) indicate that the coupling between two symmetric SRRs can widen the stop band range. However, since the two SRRs are located on either side of the middle conductor, the coupling between them is weak and a narrow passband is generated within the stop band. Meanwhile, the transmission characteristics at the higher-frequency end are worsened. Therefore, to widen the stop band and eliminate the narrow passband that may appear in this stop band, multiple SRRs can be loaded onto one side of the SSPP waveguide. To further increase this bandwidth, the resonant frequencies of the different SRRs are slightly separated by structural adjustment. In this regard, the parameter Re is used to change the ring length and the coupling capacitance of the SRRs. The rejection band can be regulated without changing the cutoff frequency of the waveguide and the external dimensions of the split rings.

The inset of Fig. 7 shows the final structure with multiple SRRs loaded onto the same side of the waveguide. Beginning at the seventh period cell in area III, nine split rings are applied with their Re increasing uniformly from 0.3 mm to 2.7 mm in steps of 0.3 mm. The other parameters are completely consistent with those of the waveguide with only a single ring.

Figure 7 also shows the simulated scattering parameters of the SSPP waveguide without SRRs and the measured S -parameters of the waveguide loaded with multiple SRRs. For the band-rejecting structure, it can be seen that the stop band of S_{21} at less than -10 dB is 5.95–7.13 GHz, and the relative bandwidth is 18%. Moreover, there is a good rectangular

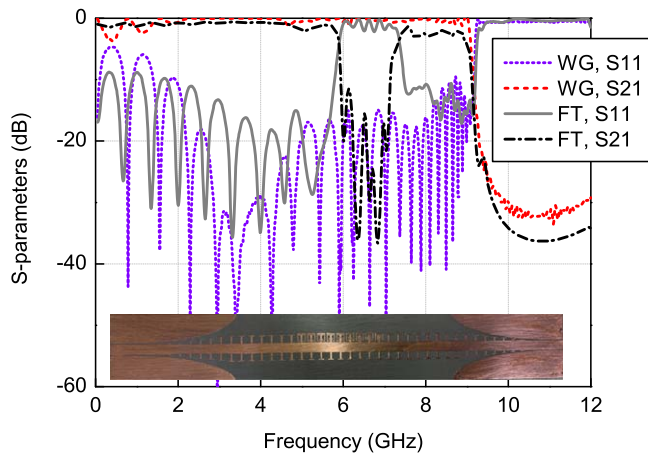


Fig. 7. (Color online) The simulated scattering characteristics of the pure SSPP waveguide (WG) and the measured S -parameters of the broad stop band filter (FT) loaded with multiple SRRs.

coefficient for this band. Meanwhile, the transmission characteristics at the low-frequency end are optimized, compared to the SSPP waveguide, but those at the high-frequency end are degraded. Obviously, this performance difference is caused by common-side SRRs. In fact, we also tested the band-rejection characteristics of the waveguide with multiple SRRs on both sides, and observed that the transmission performance was worsened (for conciseness, the results are also not shown here).

In summary, by controlling the length of the top lateral conductor, the SSPP waveguide based on T-shaped branches can easily adjust the cutoff frequency while keeping the waveguide width unchanged. This adjustment satisfies the comprehensive consideration of the field confinement and the transmission loss. When a single opening ring is loaded onto the T-shaped branch to form an SRR, a narrow stop band is achieved. The introduction of multiple opening rings with various coupling segment lengths on one side of the SSPP waveguide can achieve a broad stop band with a good rectangular coefficient. The proposed structure also has a

small lateral size, which is of benefit for the miniaturization of microwave circuits.

Acknowledgments This work was supported in part by the Natural Science Foundation of Fujian Province of China (No. 2019J01045) and in part by the National Natural Science Foundation of China (No. 62071403).

ORCID iDs Weiwen Li  <https://orcid.org/0000-0003-3545-6430>

- 1) W. L. Barnes, A. Dereux, and T. W. Ebbesen, *Nat.* **424**, 824 (2003).
- 2) Y. Fainman, K. Tetz, R. Rokitski, and P. Lin, *Opt. Photo. News* **17**, 24 (2006).
- 3) J. B. Pendry, A. J. Holden, D. J. Robbins, and W. J. Stewart, *J. Phys. Condens. Matter* **10**, 4785 (1998).
- 4) J. G. Rivas, *Nat. Photonics* **2**, 137 (2008).
- 5) J. B. Pendry, L. Martin-Moreno, and F. J. Garcia-Vidal, *Science* **305**, 847 (2004).
- 6) F. J. Garcia-Vidal, L. Martin-Moreno, and J. B. Pendry, *J. Opt. A: Pure Appl. Opt.* **7**, S97 (2005).
- 7) B. Xu, Z. Li, L. Liu, J. Xu, C. Chen, P. Ning, X. Chen, and C. Gu, *Opt. Lett.* **40**, 4683 (2015).
- 8) B. Ren, W. Li, Z. Qin, Y. Wang, L. Zhang, and B. Zhang, *Plasmonics* **15**, 551 (2020).
- 9) D. Tian, R. Xu, G. Peng, J. Li, Z. Xu, A. Zhang, and Y. Ren, *IEEE Antennas Wireless Propag. Lett.* **17**, 837 (2018).
- 10) X. Gao, J. H. Shi, X. Shen, H. F. Ma, W. X. Jiang, L. Li, and T. J. Cui, *Appl. Phys. Lett.* **102**, 151912 (2013).
- 11) X. Shen, T. J. Cui, D. Martin-Cano, and F. J. Garcia-Vidal, *Proc. Natl Acad. Sci.* **110**, 40 (2013).
- 12) Y. Chen, Z. Song, Y. Li, M. Hu, Q. Xing, Z. Zhang, L. Chai, and C.-Y. Wang, *Opt. Exp.* **14**, 13021 (2006).
- 13) X. Liu, Y. Feng, B. Zhu, J. Zhao, and T. Jiang, *Opt. Exp.* **21**, 31155 (2013).
- 14) X. Liu, Y. Feng, K. Chen, B. Zhu, J. Zhao, and T. Jiang, *Opt. Exp.* **22**, 20107 (2014).
- 15) H. F. Ma, X. Shen, Q. Cheng, W. X. Jiang, and T. J. Cui, *Laser Photonics Rev.* **8**, 146 (2014).
- 16) X. Gao, J. H. Shi, H. F. Ma, W. X. Jiang, and T. J. Cui, *J. Phys. D: Appl. Phys.* **45**, 505104 (2012).
- 17) A. P. Hibbins, B. R. Evans, and J. R. Sambles, *Science* **308**, 670 (2005).
- 18) H. C. Zhang, Q. Zhang, J. F. Liu, W. Tang, Y. Fan, and T. J. Cui, *Sci. Rep.* **6**, 23396 (2016).
- 19) E. J. Denlinger, *IEEE Trans. Microw. Theory Tech.* **MTT-28**, 513 (1980).
- 20) J. D. Baena et al., *IEEE Trans. Microw. Theory Tech.* **53**, 1451 (2005).
- 21) D. R. Smith, W. J. Padilla, D. C. Vier, S. C. Nemat-Nasser, and S. Schultz, *Phys. Rev. Lett.* **84**, 4184 (2000).
- 22) J. B. Pendry, A. J. Holden, D. J. Robbins, and W. J. Stewart, *IEEE Trans. Microw. Theory Tech.* **47**, 2075 (1999).